ELSEVIER

Computer Physics Communications 108 (1998) 147–158

Computer Physics Communications

Applications of semi-implicit Fourier-spectral method to phase field equations

L.Q. Chen [a], Jie Shen [b]

[a] *Department of Materials Science and Engineering, The Pennsylvania State University, University Park, PA 16802, USA*
[b] *Department of Mathematics, The Pennsylvania State University, University Park, PA 16802, USA*

Received 29 April 1997; revised 26 September 1997

Abstract

An efficient and accurate numerical method is implemented for solving the time-dependent Ginzburg–Landau equation and the Cahn–Hilliard equation. The time variable is discretized by using semi-implicit schemes which allow much larger time step sizes than explicit schemes; the space variables are discretized by using a Fourier-spectral method whose convergence rate is exponential in contrast to second order by a usual finite-difference method. We have applied our method to predict the equilibrium profiles of an order parameter across a stationary planar interface and the velocity of a moving interface by solving the time-dependent Ginzburg–Landau equation, and compared the accuracy and efficiency of our results with those obtained by others. We demonstrate that, for a specified accuracy of 0.5%, the speedup of using semi-implicit Fourier-spectral method, when compared with the explicit finite-difference schemes, is at least two orders of magnitude in two dimensions, and close to three orders of magnitude in three dimensions. The method is shown to be particularly powerful for systems in which the morphologies and microstructures are dominated by long-range elastic interactions. © 1998 Elsevier Science B.V.

PACS: 68.35-p; 68.35Rh
1991 MSC: 35A40; 65M70
Keywords: Phase-field; Interface motion; Semi-implicit; Fourier-spectral method

1. Introduction

There has been increasing interest in the last few years in using the diffuse-interface phase-field approach for modeling the mesoscale morphological pattern formation and interface motion, see, for example, [1] and the references therein. Typical examples include domain growth in a quenched system, crystal growth during solidification and vapor-phase deposition, morphological evolution in two-phase coherent systems, and grain growth in single-phase and two-phase systems. In the field approach, a given microstructure is specified by using a set of spatially inhomogeneous field variables, or order parameters. The temporal evolution of these field variables, and thus the temporal microstructural evolution, is described by systems of time-dependent Ginzburg–Landau (TDGL) equations and Cahn–Hilliard (CH) equations. Since both the TDGL and CH equations are nonlinear, they can only be solved numerically through discretization in space and time. Due to its simplicity and small memory requirement, most of the existing phase-field simulations employed the explicit forward Euler method in time and finite-difference in

PII S0010-4655(97)00115-X

space. To maintain the stability and to achieve high accuracy for the solutions, the time step and spatial grid size have to be very small, which seriously limits the system size and time duration of a simulation. The ability to performing reliable long-time simulation is critical in the fundamental understanding of the scaling behavior of morphological pattern evolution.

In this paper, we implement an accurate and efficient semi-implicit Fourier-spectral method for solving the phase-field equations. For the time variable, we propose to employ semi-implicit schemes in which the principal elliptic operator is treated implicitly to reduce the associated stability constraint, while the nonlinear terms are still treated explicitly to avoid the expensive process of solving nonlinear equations at each time step. Thus, at each time step, we have to deal with a constant-coefficient elliptic problem which, in the case of periodic boundary conditions, can be solved efficiently and accurately by the Fourier-spectral method whose convergence rate is exponential (for smooth functions) as opposed to second order by a usual finite-difference method. This method enjoys the following advantages over the conventional explicit Euler finite-difference method:

- Thanks to the exponential convergence of the Fourier-spectral discretization, it requires a significantly smaller number of grid points to resolve the solution to within a prescribed accuracy, say 1%. We refer to [2] for more details.
- High-order semi-implicit treatment in time enables us to use considerably larger time step size while maintaining higher accuracy.

It should be noted that the numerical scheme used in this paper, a combination of a Fourier-spectral method with backward difference schemes, has previously been employed in many different contexts, see, for instance, the books [2] and [3] and the references therein. However, to the best of our knowledge, this particular numerical scheme had not previously been applied to the phase-field equations, although a somewhat related approach was considered in [4] and [5].

In the next section, we will present our method and point out the main differences with commonly used methods. In Section 3, we will apply our schemes to predict the equilibrium profiles of an order parameter across a stationary planar interface and the velocity of a moving interface, for which the accuracy of results can be easily determined. We will compare the accuracy and efficiency of our results with those obtained by the commonly used explicit Euler finite-difference scheme. We will also apply our method to an example on strain-induced morphological transformation in two-phase systems, for which our method is shown to be particularly advantageous over real-space methods since the elasticity problem for an elastically homogeneous system has an analytical solution in Fourier space. Some concluding remarks are presented in the last section.

2. Semi-implicit Fourier-spectral method

To fix the idea, let us first consider the TDGL equation in reduced units which is written as

$$\frac{\partial \eta}{\partial t} = f(\eta) + \nabla^2 \eta \,, \tag{1}$$

subjected to the periodic boundary conditions and appropriate initial condition, where t is the time in reduced unit, the unknown η is a nonconserved order parameter, and $f(\eta) = -\eta(\eta-1)(\eta+1)$ for a simple double-well local free energy density function.

2.1. Explicit Euler finite-difference method

In the two-dimensional case, the Laplacian operator in (1) can be discretized by using either a second-order five-point or fourth-order nine-point finite-difference approximation. For a five-point approximation at a given time step n, we set

$$\nabla_h^2 \eta_i^n = \frac{1}{(\Delta x)^2} \sum_j (\eta_j^n - \eta_i^n) \,, \tag{2}$$

where $h = \Delta x$ is the spatial grid size and j represents the set of first nearest neighbors of i in a square grid. The explicit Euler finite-difference scheme can then be written as

$$\eta_i^{n+1} = \eta_i^n + \Delta t \left[(f(\eta^n))_i + \nabla_h^2 \eta_i^n \right] \,, \tag{3}$$

where Δt is the time step size. The above scheme is the most often used scheme in numerical simulations of the TDGL or Cahn–Hilliard equations (see, for instance, [6–10]).

It is well known (see, for instance, [11]) that the above scheme, and other higher-order explicit schemes, have a time step constraint dictated by

$$\Delta t \approx (\Delta x)^2 , \tag{4}$$

which is the consequence of explicit treatment of the Laplacian operator. Thus, with the second-order five-point finite-difference approximation, there is no advantage to use a higher-order explicit scheme for which the time step is still restricted by (4). This remark and its extreme simplicity are the main reasons why the explicit Euler finite-difference scheme is widely used in practice. However, for relatively simple equations in simple geometries as we are interested here, it is possible to develop much more efficient numerical schemes. We will present below a semi-implicit Fourier-spectral method which is capable of providing significantly more accurate results with less grid points and larger time step size.

It should be noted that an explicit scheme for the CH equation has a much severer time step constraint dictated by (see, for instance, [11])

$$\Delta t \approx (\Delta x)^4 , \tag{5}$$

which is the consequence of explicit treatment of the biharmonic operator in the CH equation. This condition will become prohibitively restrictive for small grid sizes and for three-dimensional problems.

2.2. *Semi-implicit Fourier-spectral method*

Instead of using a finite-difference approximation, we propose to use a Fourier-spectral approximation to (1) by transforming the partial differential equation into a sequence of ordinary differential equations in the Fourier space

$$\frac{d}{dt}\tilde{\eta}(\boldsymbol{k},t) = \{\tilde{f}(\eta)\}_{\boldsymbol{k}} - k^2\tilde{\eta}(\boldsymbol{k},t) , \tag{6}$$

where $\boldsymbol{k} = (k_1, k_2)$ is a vector in the Fourier space, $k = \sqrt{k_1^2 + k_2^2}$ is the magnitude of $\boldsymbol{k}$, $\tilde{\eta}(\boldsymbol{k},t)$ and $\{\tilde{f}(\eta)\}_{\boldsymbol{k}}$ represent the Fourier transforms of $\eta(x,t)$ and $f(\eta)$, respectively. Thus, the explicit Euler Fourier-spectral method is to approximate the above equations by the explicit Euler scheme

$$\tilde{\eta}^{n+1}(\boldsymbol{k}) = \tilde{\eta}^n(\boldsymbol{k}) + \Delta t\left[\{\tilde{f}(\eta^n)\}_{\boldsymbol{k}} - k^2\tilde{\eta}^n(\boldsymbol{k})\right] . \tag{7}$$

This scheme has been extensively used in numerical simulations of systems involving long-range interactions such as long-range elastic and coulombic interactions for which analytical expressions exist in Fourier space (see [12,13]). Unfortunately, although this scheme provides excellent spatial accuracy, it is only first-order accurate in time and suffers from the same very restrictive time step constraint (4) with $\Delta x = T/N$, where T is the period of the function and N is the number of grid points in one direction.

To remove the shortcoming with the small time step size associated with the explicit Euler scheme, we proposed the following semi-implicit scheme:

$$(1 + \Delta t k^2)\tilde{\eta}^{n+1}(\boldsymbol{k}) = \tilde{\eta}^n(\boldsymbol{k}) + \Delta t\{\tilde{f}(\eta^n)\}_{\boldsymbol{k}} ,$$
$$-\tfrac{1}{2}N + 1 \le k_1 , \quad k_2 \le \tfrac{1}{2}N , \tag{8}$$

where N is the number of grid points in one direction. To reduce the computational cost, the nonlinear term $\{\tilde{f}(\eta^n)\}_{\boldsymbol{k}}$ should be evaluated by using the so-called transform method developed by Orszag (see, for instance, [2]).

It will be shown below that we can increase the time step size by about 10 times (assuming $\Delta x = 1.0$) by using semi-implicit scheme (8) as compared to the explicit one (7), yet still maintain the spatial accuracy of the Fourier-spectral method. The increase in time step size would become about 100 times if we reduce the spatial grid size from 1.0 to 0.25. Therefore, scheme (8) is the ideal choice if one is mainly interested in the final equilibrium solution, e.g. in the equilibrium shape of a domain. However, it should be emphasized that (8) is still only first-order accurate in time, and hence is not sufficient if one is interested in time-dependent solutions. The accuracy in time can be significantly improved by using higher-order semi-implicit schemes. For instance, a second-order backward difference (BDF) for $(d/dt)\tilde{\eta}$ and a second-order Adams–Bashforth (AB) for the explicit treatment of nonlinear term applied to (6) lead to the following second-order BDF/AB scheme:

$$(3 + 2\Delta t k^2)\tilde{\eta}^{n+1}(\boldsymbol{k}) = 4\tilde{\eta}^n(\boldsymbol{k}) - \tilde{\eta}^{n-1}(\boldsymbol{k})$$
$$+2\Delta t\left[2\{\tilde{f}(\eta^n)\}_{\boldsymbol{k}} - \{\tilde{f}(\eta^{n-1})\}_{\boldsymbol{k}}\right] . \tag{9}$$

We may use (8) to compute $\tilde{\eta}^1$, and hence $\tilde{f}(\eta^1)$, which are needed to start the iteration in (9).

We can also construct a third-order semi-implicit BDF/AB scheme,

$$(11 + 6\Delta t k^2)\tilde{\eta}^{n+1}(\boldsymbol{k}) = 18\tilde{\eta}^{n}(\boldsymbol{k}) - 9\tilde{\eta}^{n-1}(\boldsymbol{k}) + 2\tilde{\eta}^{n-2}(\boldsymbol{k}) + 6\Delta t\Big[3\{\tilde{f}(\eta^{n})\}_{\boldsymbol{k}} - 3\{\tilde{f}(\eta^{n-1})\}_{\boldsymbol{k}} + \{\tilde{f}(\eta^{n-2})\}_{\boldsymbol{k}}\Big]. \tag{10}$$

To start the iteration in (10), we may use respectively (8) and (9) to compute $\tilde{\eta}^1$ and $\tilde{\eta}^2$.

Similar semi-implicit schemes of fourth-order or higher can also be constructed, but our experiences suggest that the second- and third-order schemes above usually provide the best accuracy/cost ratio. For many problems of interest, the second-order scheme is sufficiently accurate.

It can be shown, and is verified by our numerical experiments (see Table 2), that the above schemes are unconditionally stable in the sense that for a fixed set of physical parameters there exists a critical Δt_c, independent of the spatial grid size, such that for all $\Delta t \leq \Delta t_c$, the above schemes are stable for all spatial grid sizes. Thus we may choose time step size much larger than that allowed by an explicit scheme.

Similar schemes can be designed for the fourth-order Cahn–Hilliard equation

$$\frac{\partial c}{\partial t} = -\nabla^2(f(c) + \nabla^2 c)\,, \tag{11}$$

where c is a conserved order parameter, usually the local composition for a binary system. By using the Fourier-spectral method for the spatial variables, and, treating the linear fourth-order operators implicitly and the nonlinear terms explicitly, the first-order semi-implicit Fourier-spectral scheme is

$$(1 + \Delta t k^4)\tilde{c}^{n+1}(\boldsymbol{k}) = \tilde{c}^{n}(\boldsymbol{k}) + \Delta t k^2\{\tilde{f}(c^n)\}_{\boldsymbol{k}}\,. \tag{12}$$

A corresponding second-order BDF/AB scheme is

$$(3 + 2\Delta t k^4)\tilde{c}^{n+1}(\boldsymbol{k}) = 4\tilde{c}^{n}(\boldsymbol{k}) - \tilde{c}^{n-1}(\boldsymbol{k}) + 2\Delta t k^2\left[2\{\tilde{f}(c^n)\}_{\boldsymbol{k}} - \{\tilde{f}(c^{n-1})\}_{\boldsymbol{k}}\right]. \tag{13}$$

Our preliminary numerical simulations indicate that by going from explicit to semi-implicit, the time step can be increased by two to three orders of magnitude.

Note that Copetti and Elliott [14] recently proposed a semi-implicit finite-difference method for solving the CH equation as applied to the kinetics of spinodal decomposition. In their scheme, the CH equation was first discretized using a second-order five-point finite-difference approximation, and then transformed to the Fourier space. Using their scheme, the TDGL equation becomes

$$\frac{d}{dt}\tilde{\eta}(\boldsymbol{k}, t) = \{\tilde{f}(\eta)\}_{\boldsymbol{k}} - \lambda(\boldsymbol{k})\tilde{\eta}(k, t)\,, \tag{14}$$

where

$$\lambda(\boldsymbol{k}) = \left(2\cos(2\pi k_x + 2\cos(2\pi k_y) - 4\right)/(\Delta x)^2\,,$$

with $\boldsymbol{k} = (k_x, k_y) = (k_1/N_x, k_2/N_y)$, where N_x and N_y are respectively the number of grid points along the x and y directions. They then discretized the above equation using a first-order semi-implicit scheme in time. It should be noted that although (14) and (6) appear to be similar, they are fundamentally different because the spatial discretization error of (14) is still second order due to the finite-difference approximation.

3. Numerical simulations and discussions

In order to compare the accuracy and stability of the proposed semi-implicit Fourier-spectral method with other commonly used schemes, we calculated an one-dimensional equilibrium profile across a stationary flat interface and studied the shrinkage kinetics of a two-dimensional circular domain. For both examples, the exact solutions can be obtained and the accuracy of numerical solutions can be reliably assessed. To demonstrate the application, we also present a numerical simulation of strain-induced morphological evolution in two-phase systems.

3.1. The equilibrium profile

We consider the TDGL equation (1) in one dimension. The system size is 128 in reduced units. At $t = 0$, half of the grid points are assigned a value of $+1$ and the other half -1. Since we applied periodic boundary conditions, there are two interfaces which separate regions with $\eta = +1$ and -1: one is at the origin and one at $x = 64$. It is found that, with a system size of 128, the two interfaces are sufficiently far apart and they do not interact, i.e. the order parameter profile

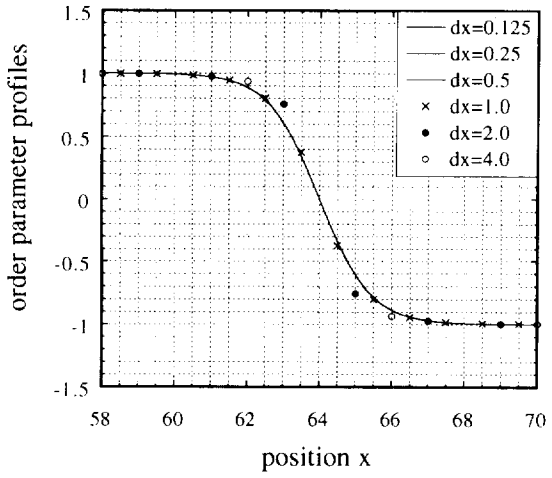

Fig. 1. Equilibrium profiles across a stationary planar interface obtained from the finite-difference method for various grid sizes ranging from $\Delta x = 0.125$ to 4.0.

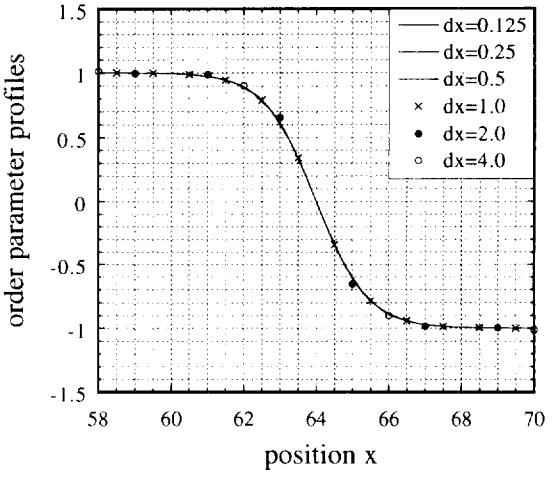

Fig. 2. Equilibrium profiles across a stationary planar interface obtained from the spectral method for various grid sizes ranging from $\Delta x = 0.125$ to 4.0.

across an interface is not affected by the presence of a second interface in the system.

It is obvious that the equilibrium profile is the same and independent of the time step size, whether one uses an explicit or the implicit method. However, the accuracy of the equilibrium profile obtained from the numerical computation does depend on the spatial grid size and on the accuracy of the spatial discretization scheme. Therefore, we just need to compare the profiles obtained from the finite-difference discretization scheme and the spectral method. The equilibrium profiles obtained from the finite-difference scheme (3) and from the spectral method (8), are shown in Figs. 1 and 2, respectively, for various grid sizes ranging from $\Delta x = 0.125$ to 4.0. Figs. 1 and 2 display only part of the profile associated with the interface at $x = 64$. In Fig. 3, we compare the profiles obtained from the finite-difference method and the spectral method at $\Delta x = 0.25$. Notice that the profiles are visually the same, indicating that both methods provide satisfactory results at $\Delta x = 0.25$. We then compare the profiles from the two methods for $\Delta x = 1.0$ in Fig. 4. One may notice that all the data points obtained from the spectral method are still very close to the accurate equilibrium profile (obtained with $\Delta x = 0.01$), whereas the four data points within the interfacial region obtained from the finite-difference method are noticeably different.

In order to have a better idea on the accuracy obtained from the two methods, we estimated the errors for the data points within the interfacial region for a number of different grid sizes (Table 1). We assumed that the values obtained from the spectral method with $\Delta x = 0.01$ are as accurate.

Table 1
Comparison of errors in calculating the order parameter profiles across an interface using finite-difference and Fourier-spectral methods

Δx	Finite-difference method	Fourier-spectral method
0.25	0.5%	0.0%
0.5	2.2%	0.0%
1.0	10.4%	0.4%
2.0	24.2%	7.6%

From Table 1, it is clear that $\Delta x = 1.0$ is more than sufficient to achieve an accuracy of 0.5% using the spectral method. On the other hand, to achieve the same spatial accuracy using the finite-difference scheme, Δx has to be reduced to 0.25 or smaller, i.e. the spatial grid size in the finite-difference scheme has to be at least four times smaller than that used in the spectral method.

Very often it is meaningful to measure the grid size in terms of the interface width which can be analytically estimated (Fig. 5) to be

$$L = 2\sqrt{2} \approx 2.8 .$$

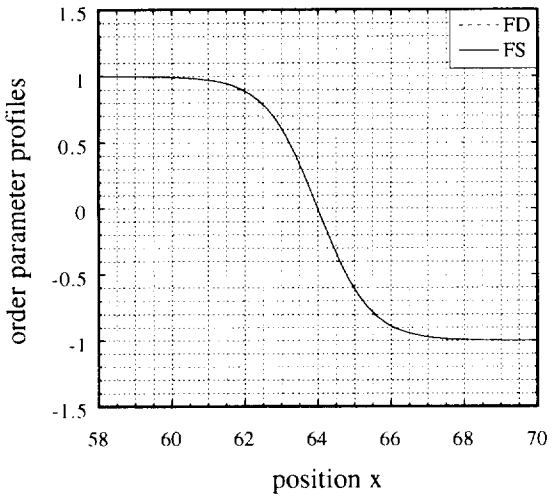

Fig. 3. Comparison of the order parameter profiles across a stationary planar interface obtained from the finite-difference (FD) method and the Fourier-spectral (FS) method both using $\Delta x = 0.25$.

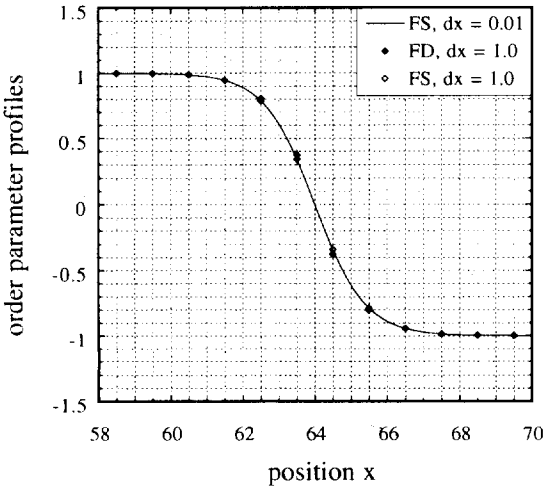

Fig. 4. Comparison of the order parameter profiles across a stationary planar interface obtained from the finite-difference (FD) method and the Fourier-spectral (FS) method both using $\Delta x = 1.0$.

Based on the estimate of the interfacial width and Table 1, one can see that the error using three grid points to resolve the interfacial region is about 0.4% in the spectral method, whereas in the finite-difference method, to achieve the same accuracy, at least twelve grid points are required to resolve the interfacial width.

We also compare the maximum size of time step that one can use in various numerical schemes in Table 2.

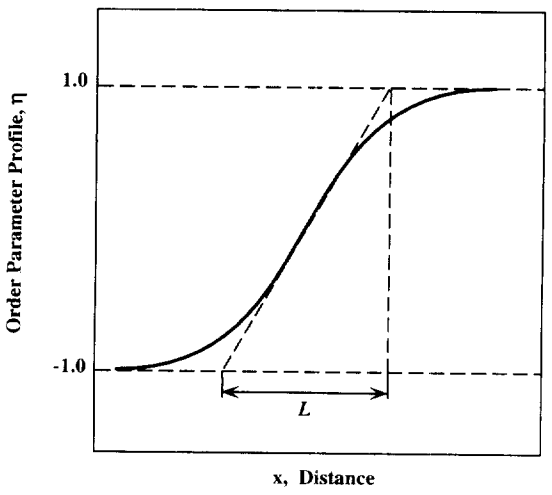

Fig. 5. A schematic order parameter profile illustrating the definition of interfacial thickness L.

Table 2
Maximum allowable time step size

Numerical scheme	Δt_{max} ($\Delta x = 1.0$)	Δt_{max} ($\Delta x = 0.25$)
Explicit Euler finite-difference	0.25	0.03
Explicit Euler Spectral	0.09	0.006
First-order semi-implicit spectral	0.9	0.9
Second-order semi-implicit spectral	0.6	0.6
Third-order semi-implicit spectral	0.4	0.4

The maximum size of time step was estimated from the numerical computations as the maximum value that one can use and still produces the same profile as those obtained using smaller size of time steps. As discussed above, in order to achieve a similar level of accuracy (e.g. 0.5%), the spatial grid size in the finite-difference method has to be at least four times smaller than that used in the spectral method. Therefore, in Table 2, we compare the maximum time step size for two different spatial grid sizes, $\Delta x = 1.0$ and 0.25. According to Table 2, reducing the spatial grid size from 1.0 to 0.25, the corresponding time step size has to be reduced by about 10 times in the two explicit schemes. On the other hand, in the semi-implicit schemes, the same time step size could be used with the two different spatial grid sizes.

It is clear that semi-implicit schemes allow much larger time step sizes than explicit schemes do, and that higher-order semi-implicit schemes are slightly

Table 3
Relative CPU per time step with a fixed number of grid points

Numerical scheme	Relative CPU
Explicit Euler finite-difference	1.0
Explicit Euler spectral	1.26
Semi-implicit finite-difference	1.26
First-order semi-implicit spectral	1.26
Second-order semi-implicit spectral	1.39
Third-order semi-implicit spectral	1.46

less stable than lower-order semi-implicit schemes.

In Table 3, we list the relative computational times for each time step using different schemes, normalized by the value corresponding to the explicit Euler finite-difference scheme ($\approx$ 7.9E−3 second for each time step with a 256 × 256 2D lattice run on Cray C90). The Fourier transforms were performed using the Fast Fourier Transform routines on Cray C90. Notice that the semi-implicit spectral schemes only cost 25% to 45% more per time step (with the same number of grid points) than the explicit Euler finite-difference schemes, but provide significantly more accurate results and allow much larger time steps. Combining the results in Tables 1, 2 and 3, we can roughly estimate the improvement on computational efficiency using a semi-implicit spectral method relative to the explicit Euler finite-difference scheme. To solve a 2D TDGL system with an accuracy of about 0.5%, the relative speedup for using the second-order semi-implicit scheme is $4 \times 4 \times 0.6 \div 0.03 \div 1.39 \approx 230$. For a 3D system, the speedup would be ≈ 920.

3.2. *The velocity of a circular moving interface*

In order to predict quantitatively the kinetics of microstructural evolution, one has to calculate not only the accurate equilibrium profiles but also the accurate velocity of a moving interface. To compare the accuracy of various schemes, we consider the TDGL equation (1) in two dimensions and a system size 256 × 256 (in reduced units). At $t = 0$, there is a circular interface boundary with a radius of 100. The order parameter values inside the circle are assigned +1 and −1 outside. Such a circular interface is unstable and the driving force for its motion is the mean curvature. Therefore, the circle will shrink and eventually disappear (Fig. 6). It can easily be shown that, in the limit that the radius of the circle is much larger than the interfacial thickness, the velocity of the moving interface, V, is given by (see [15])

$$V = \frac{dR}{dt} = -\frac{1}{R}, \tag{15}$$

where R is the radius of the circle at a given time t. The negative sign indicates the interface moves towards its center of curvature. Integrating (15), we find

$$R_0^2 - R^2 = 2t, \tag{16}$$

where R_0 is the initial radius size, or

$$A = A_0 - 2\pi t, \tag{17}$$

where A is the area of the circle at time t and A_0 is the initial area.

The areas of a circle as a function of time obtained from different numerical schemes are shown in Fig. 7 using time step size $\Delta t = 0.25$, which is the maximum value that one can use to avoid numerical instability for the explicit Euler finite-difference scheme. The grid size, Δx, is chosen to be 1.0. The area of the circle is calculated by counting the total number of grid points at which the order parameter values are larger than 0. The explicit spectral scheme was not included in Fig. 7, since, with this time step size, it is unstable. As we can see from Fig. 7, all the schemes result in a linear dependence of the area on time. However, the slopes of the lines are quite different. The thick solid line labeled as "theory" is a plot of Eq. (14) with a slope of 2π. We may characterize the accuracy of different schemes by comparing the slopes of the lines with the analytical Eq. (14). The resulting errors are shown in the third column of Table 4. Notice that, with this time step size, the semi-implicit finite-difference scheme leads to the worst accuracy as compared to the analytical result with an error of $\approx$ 18%. On the other hand, there is no visible difference between the numerical results obtained from the second-order semi-implicit spectral method and the analytical solution on the sharp-interface limit (error $\approx$ 0.033%). The errors from the explicit Euler finite-difference scheme and the semi-implicit spectral scheme are similar ($\sim$ 9.1–9.2%) and somewhere in-between those obtained from the semi-implicit finite-difference scheme and the second-order semi-implicit spectral method. One may notice that, with the finite-difference approximation, reducing the time step size from 0.25 to 0.05 does

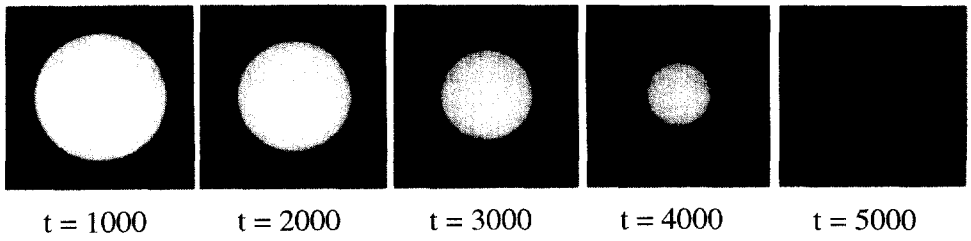

Fig. 6. Temporal evolution of a circular domain.

not improve the accuracy significantly (from 9.2% to 9.1%) due to the limitation of the spatial resolution. On the other hand, with the spectral method, the predicted interface kinetics is very accurate if a small enough time step size is employed (error ≈ 0.028 % with $\Delta t = 0.05$). In order to further improve the accuracy of solution using the finite-difference approximation, the grid size Δx must be reduced (by about four times according to the last section). The dependence of the areas of a circular domain on time from different semi-implicit schemes are shown in Figs. 8 and 9 for $\Delta t = 0.5$ and $\Delta t = 0.9$, respectively. The corresponding errors in the slopes, and hence in the velocities, are listed in Table 3. Among the semi-implicit schemes, the finite-difference one is the worst at any size of time step and therefore the spectral method is preferred. The second-order semi-implicit spectral scheme seems to have the best accuracy/cost ratio for this problem. According to Table 4, with a moderate accuracy requirement, there appears to be very little advantage to use a third-order semi-implicit spectral method. However, it may become preferable for problems with high accuracy requirement.

3.3. Strain-dominated microstructure evolution

To demonstrate the wide applicability of the semi-implicit Fourier-spectral method, we consider the microstructure evolution in elastically homogeneous coherent two-phase solids using the Cahn–Hilliard equation (11). In coherent systems, one of the main contributions to the total driving force for microstructure evolution is the elastic strain energy caused by the lattice mismatch between the two phases. It is safe to assume that the mechanical equilibrium in a system is established much faster than any diffusion processes. As a result, the system is always at mechanical equilibrium during phase separation or during coarsening.

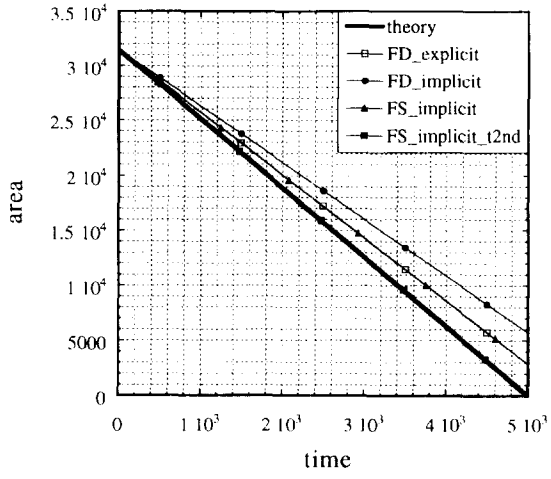

Fig. 7. Areas of a circular domain as a function of time obtained from different numerical schemes using a time step size $\Delta t = 0.25$. FD: finite-difference; FS: Fourier-spectral.

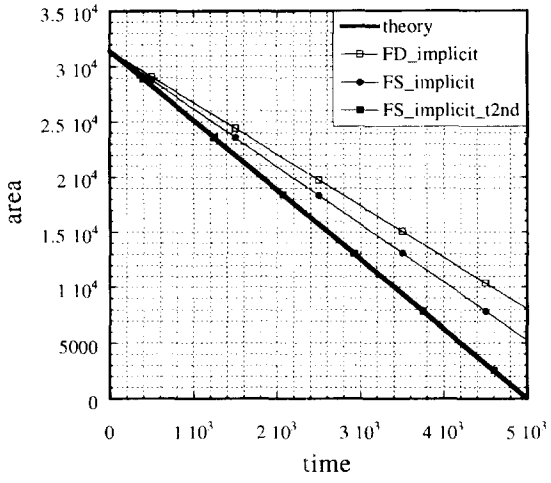

Fig. 8. Areas of a circular domain as a function of time obtained from different numerical schemes using a time step size $\Delta t = 0.5$. FD: finite-difference; FS: Fourier-spectral.

Table 4
The errors in the slopes of the area dependence of a circular domain

Schemes	$\Delta t = 0.05$	$\Delta t = 0.25$	$\Delta t = 0.5$
Explicit Euler finite-difference	9.1%	9.2%	not stable
Explicit Euler spectral	0.028%	not stable	not stable
Semi-implicit finite-difference		18.1%	25.5%
First-order semi-implicit spectral		9.1%	16.7%
Second-order semi-implicit spectral		0.033%	0.033%
Third-order semi-implicit spectral		0.033%	not reliable

Therefore, at each time step, the mechanical equilibrium equations have to be solved either numerically or analytically. It was shown by Khachaturyan [16] that, in the homogeneous modulus approximation, the elastic energy of any arbitrary microstructure can be analytically calculated. However, the elastic energy is a double-volume integral of infinitely long-ranged elastic interactions in real space, and its contribution to the total driving force enters the right-hand side of Eq. (11) as a volume integral, a nonlocal term. Therefore, direct numerical solution of the CH equation (11) in real space is prohibitively difficult. In Fourier space, the elastic energy is reduced to a single volume integral of the Fourier transform of the elastic interactions and its contributions enters CH equation as a single term. For example, for the first-order implicit scheme (12), it becomes

$$(1 + \Delta t k^4)\tilde{c}^{n+1}(\boldsymbol{k}) = \tilde{c}^n(\boldsymbol{k})(1 + B(\boldsymbol{e})) + \Delta t k^2 \{\tilde{f}(c^n)\}_{\boldsymbol{k}}, \tag{18}$$

where $\boldsymbol{e}$ is a unit vector in Fourier space and $B(\boldsymbol{e})$ is the Fourier transform of the long-range elastic interactions. For a cubic two-phase solid and assuming that the lattice parameter difference between the two phases is directly proportional to their compositional difference, i.e., Vegard's law, in a two-dimensional model, $B(\boldsymbol{e})$ is given by [17,12]

$$B(\boldsymbol{e}) \cong B_{\mathrm{el}} e_x^2 e_y^2, \tag{19}$$

where e_x and e_y are the x and y components of the unit vector $\boldsymbol{e}$, and B_{el} is a material constant which depends on the elastic constants and misfit strain. A positive value for B_{el} represents a system with negative elastic anisotropy. It is clear from Eq. (18) that the elastic energy contribution to the total driving force does not complicate the numerical solution of CH equation in the Fourier-spectral method.

An example of microstructural evolution obtained from Eq. (18) is shown in Fig. 9. The system size is 2048×2048 in reduced units with periodic boundary conditions along both x and y directions. The real space grid size, Δx, is equal to 1.0 and time step Δt is chosen to be 2.0 although as large as 2.5 can be used. The parameter B_{el} is set to 2.0. The nonlinear function, $f(c)$, is given by

$$f(c) = c(1 - c)(1 + c), \tag{20}$$

which produces equilibrium compositions at -1.0 and $+1.0$ in the absence of elastic interactions. The initial condition is a homogeneous composition distribution plus small random perturbations, i.e. at $t = 0$,

$$c(\boldsymbol{r}) = c_o + \zeta(\boldsymbol{r}), \tag{21}$$

where c_o is the average composition which is chosen to be 0, and hence the volume fractions of the resultant two phases are 50% each. $\zeta(\boldsymbol{r})$ is a small random perturbation at each grid necessary to evolve the initial homogeneous state. The gray levels in Fig. 9 represent the magnitude of c at each grid point in real space. As one would expect, the initially homogeneous phase separates into regions of low and high compositions followed by coarsening of the composition domains (Fig. 9). The strong alignment of the composition domains along the x and y directions is entirely due to the long-range elastic interactions since the interfacial energy is isotropic. For a cubic alloy with negative elastic anisotropy, x and y directions are elastically soft directions and morphological alignment along those directions results in decreases in the elastic energy. Just for comparison, the morphological evolution in the same system but without the elastic

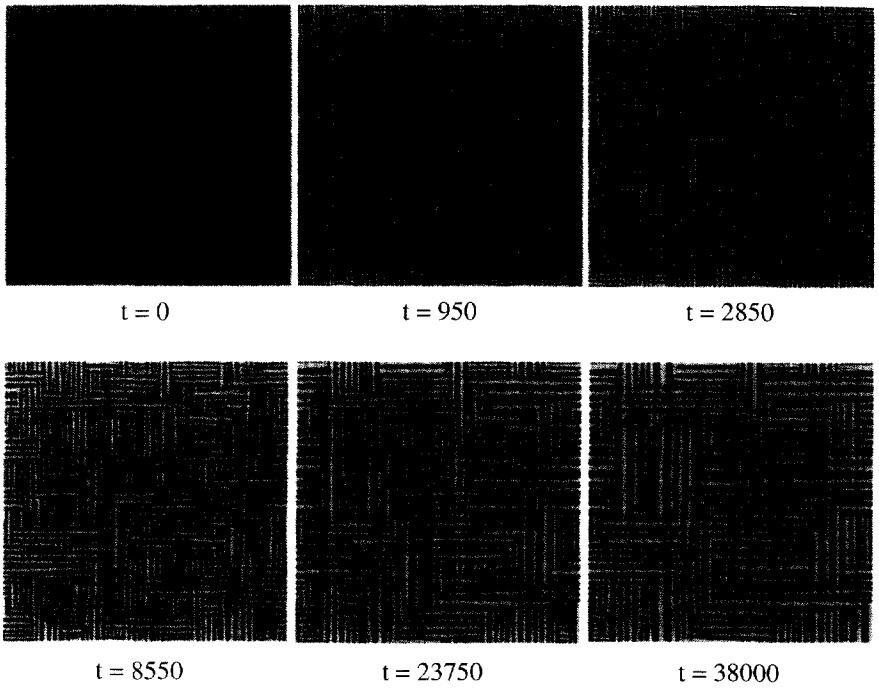

Fig. 9. Temporal evolution of strain-dominated morphological patterns during a spinodal decomposition and subsequent coarsening.

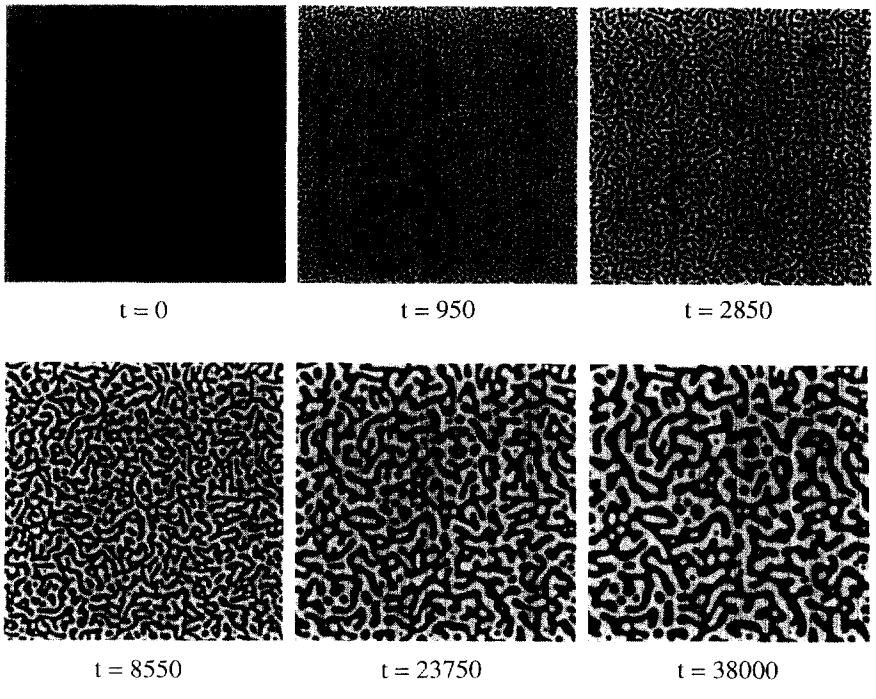

Fig. 10. Temporal evolution of morphological patterns during spinodal decomposition and subsequent coarsening without the elastic strain effect.

interactions is shown in Fig. 10. To determine the efficiency of the semi-implicit method, we also performed numerical simulations of the Cahn–Hilliard equation using the explicit Fourier-spectral method. We found that the maximum time step that one can use without developing numerical instability is 0.005 which is about 400–500 times smaller than that can be used in the first-order semi-implicit method. In most previous numerical simulations of strain-induced morphological evolution, the explicit method was employed, see the review article [18]. We also tested the second-order BDF/AB scheme (13). The maximum time step that we can use is 0.4 which is about 5 times smaller than the first-order scheme. Our preliminary results show that, for this particular problem, the difference in obtained results on domain growth kinetics from the first- and second-order schemes is on the same order of magnitude as the differences arising from different set of initial random perturbations, $\zeta(\boldsymbol{r})$, introduced to the initial homogeneous state, which seems to indicate that the first-order scheme already provides sufficient accuracy. For more general cases of using Cahn–Hilliar equation to predict time-dependent quantities, the accuracies of first- and higher-order schemes remain to be studied.

4. Concluding remarks

We introduced an efficient and accurate numerical scheme, the semi-implicit Fourier-spectral method, for solving the TDGL equation and CH equation.

For a single TDGL equation, it is demonstrated that for a prescribed accuracy of 0.5% in both the equilibrium profile of an order parameter and the interface velocity, the semi-implicit Fourier-spectral method is about 200 and 900 times more efficient than the explicit Euler finite-difference scheme in 2D and 3D, respectively.

For a single CH equation describing the strain-dominated microstructural evolution, the time step that one can use in the first-order semi-implicit Fourier-spectral method is about 400–500 larger than the explicit Fourier-spectral method.

Although we have only considered the periodic boundary conditions here, the semi-implicit schemes can also be efficiently applied to the TDGL and CH equations with Dirichlet, Neumann or mixed boundary conditions by using the fast Legendre- or Chebyshev-spectral methods developed in [19,20] for second- and fourth-order equations. On the other hand, the proposed method has also its limitations. It is most efficient when applied to problems whose principal elliptic operators have constant coefficients, although problems with variable coefficients can be treated with slightly less efficiency, for instance, by an iterative procedure (see, e.g., [19]) or by a collocation approach (see, e.g., [3]). Also, since the proposed method uses a uniform grid for the spatial variables, it may have difficult to resolve extremely sharp interfaces with a moderate number of grid points. In this case, an adaptive spectral method may become more appropriate (see, e.g. [21]).

As a final note, it should be pointed out that many previous numerical simulations using the TDGL and CH field equations are limited by the poor efficiency and accuracy of the explicit finite-difference schemes. As a result, the growth rates of the spatial scale of a morphological or microstructural pattern predicted from such numerical simulations cannot be trusted. It is also questionable that the so-called "scaling state" of a microstructure has ever been reached in these simulations because of the limit on simulation time and system size, as pointed out by Oono very recently [22], "...an honest numerical solution of the fourth-order nonlinear partial differential equation for very long time for very large systems is still prohibitively difficult. All the published numerical results on the Cahn–Hilliard equation should be interpreted as the numerical results due to inefficient or not optimized cell-dynamics system (CDS) models". Although we feel that the latter statement might be too inclusive, but at least it indicates that many previous published numerical results were not quite reliable. By using the highly accurate and stable semi-implicit spectral methods proposed in this paper, it is now feasible to perform highly accurate numerical simulations on the TDGL and CH equations for much larger systems and for much longer time. As demonstrated in our preliminary simulations using the CH equation, the proposed spectral method is particularly powerful for studying the temporal evolution of microstructural patterns influenced by long-range interactions such as long-range elastic interactions.

Acknowledgements

This work is supported by the National Science Foundation through grant DMR-9633719 (LQC) and grant DMS-9623020 (JS), and by the Office of Naval Research Young Investigator Program under the grant number N-00014-95-1-0577 (LQC). Numerical simulations were performed at the Pittsburgh Super-computing Center.

References

[1] L.Q. Chen, Y.Z. Wang, Continuum field approach to modeling microstructural evolution, JOM 48 (1996) 13–18.
[2] D. Gottlieb, S.A. Orszag, Numerical Analysis of Spectral Methods: Theory and Applications (SIAM-CBMS, Philadelphia, PA, 1977).
[3] C. Canuto, M.Y. Hussaini, A. Quarteroni, T.A. Zang, Spectral Methods in Fluid Dynamics (Springer, Berlin, 1987).
[4] J. Strain, Fast spectrally-accurate solution of variable-coefficient elliptic problems, Proc. Am. Math. Soc. 122 (1994) 843–850.
[5] J. Strain, Spectral methods for nonlinear parabolic systems, J. Comput. Phys. 122 (1995) 1–12.
[6] O.T. Valls, G.F. Mazenko, Numerical study of the growth kinetics for a langevin equation, Phys. Rev. B 34 (1986) 7941–7950.
[7] T.M. Rogers, K.R. Elder, R.C. Desai, Numerical study of the late dsstages of spinodal decomposition, Phys. Rev. B 37 (1988) 9638–9649.
[8] A. Chakrabarti, R. Toral, J.D. Gunton, Lates stages of spinodal decomposition in a three-dimensional model system, Phys. Rev. B 39 (1989) 4386–4394.
[9] J.A. Warren, W.J. Boettinger, Prediction of dendritic growth and microsegregation patterns in a binary alloy using the phase-field method, Acta Metall. Mater. 43 (1995) 689–673.
[10] L.Q. Chen, W. Yang, Computer simulation of the dynamics of a quenched system with large number of non-conserved order parameters, Phys. Rev. B 50 (1994) 15752–15756.
[11] R.D. Richtmyer, K.W. Morton, Difference Methods for Initial Value Problems (Interscience, New York, 1976).
[12] Y. Wang, L.Q. Chen, A.G. Khachaturyan, Kinetics of strain-induced morphological transformationin cubic alloys with a miscibility gap, Acta Metall. Mater. 41 (1995) 279–296.
[13] D.N. Fan and L.Q. Chen, Possibility of spinodal decomposition in yittria-partially stabilized zirconia($zro_2 - y_2o_3$) system – a theoretical investigation, J. Am. Ceram. Soc. 78 (1995) 1680–1686.
[14] M.I.M. Copetti, C.M. Elliot, Kinetics of phase decomposition processes: Numerical soutions to Cahn-Hilliard equation, Mater. Sci. & Technol. 6 (1990) 273–283.
[15] S.M. Allen, J.W. Cahn, A microscopic theory for antiphase boundary motion and its application to antiphase domain coarsening, Acta Metall. Mater. 27 (1979) 1085–1095.
[16] A.G. Khachaturyan, Theory of Structural Transformations in Solids (Wiley, New York, 1983).
[17] L.Q. Chen, Y.Z. Wang, A.G. Khachaturyan, Transformation-induced elastic strain effect on the precipitation kinetics of ordered intermetallics, Phil. Mag. Lett. 64 (1991) 241–251.
[18] Y.Z. Wang, L.Q. Chen, A.G. Khachaturyan, Modeling of dynamical evolution of micro/mesoscopic morphological patterns in coherent phase transformations, in: Computer Simulation in Materials Science, H.O. Kirchner et al., eds. (Kluwer Academic Publishers, Dordrecht, 1996) pp. 325–371.
[19] Jie Shen, Efficient spectral-Galerkin method I. Direct solvers for second- and fourth-order equations by using Legendre polynomials, SIAM J. Sci. Comput. 15 (1994) 1489–1505.
[20] Jie Shen, Efficient spectral-Galerkin method II. Direct solvers for second- and fourth-order equations by using Chebyshev polynomials, SIAM J. Sci. Comput. 16 (1995) 74–87.
[21] A. Bayliss, R. Kuske, B.J. Matkowsky, A two-dimensional adaptive pseudo-spectral method, J. Comput. Phys. 91 (1990) 174–196.
[22] Y. Oono, Structral stability of spinodal decomposition, in: Mathematics of Microstructure Evolution, EMPMD Monograph Series 4, L.Q. Chen, B. Fultz, J.W. Cahn, J.R. Manning, J.E, Morraland, J.A. Simmons, eds. (TMS, SIAM, Philadelphia, PA, 1996) pp. 355–365.